This document was prepared in conjunction with work accomplished under Contract No. DE-AC09-96SR18500 with the U.S. Department of Energy.

**DISCLAIMER**

# FRACTURE TOUGHNESS TESTING OF ASTM A285 STEEL FOR FRACTURE ANALYSIS OF SAVANNAH RIVER SITE STORAGE TANKS

**K. H. Subramanian, A. J. Duncan, R. L. Sindelar**
Savannah River Technology Center
Westinghouse Savannah River Company
Aiken, SC 29808

**J. J. Lewandowski, C. J. Tuma**
Materials Science and Engineering
Case Western Reserve University
Cleveland, OH 44106

## ABSTRACT

The fracture toughness properties of A285 steels are being measured at specific material and test conditions for application to elastic-plastic fracture mechanics analysis of storage tanks at the Department of Energy Savannah River Site (SRS). Materials for testing were selected over ranges based on compositions that span the tank plates. Property measurements focus on J-R curve testing in order to characterize ductile fracture behavior of these materials at operational temperatures. The results show a strong loading rate effect, but minimal thickness and temperature effects in the ranges tested.

The results from compact tension fracture toughness testing suggest that the initial load carrying capacity and the initial resistance to ductile tearing increases with increasing loading rate. However, this strain rate sensitivity could lead to the unexpected onset of cleavage fracture after some amount of ductile tearing. Testing of archival material at high strain rates revealed that stable ductile tearing was interrupted by cleavage fracture.

Ongoing testing will be done to complete the test matrix to complement additional and complete microstructural analysis. The influence of each of the variables on fracture toughness as well as the occurrence of cleavage fracture will be analyzed when the testing is complete.

## INTRODUCTION

A materials test program plan was developed to measure mechanical properties of ASTM Type A285 carbon steel used to construct storage tanks at the Department of Energy Savannah River Site. Under this plan, fracture toughness and tensile testing was performed on ASTM Type A285 steels that span storage tank plate compositions. The mechanical properties will be used in the J-T methodology to ultimately discern structural integrity.

Mechanical testing is in progress as per a statistically designed test matrix. The effect of (1) chemical composition, (2) microstructure, (3) temperature, (4) orientation, and (5) loading rate are being investigated. The full data set that will be ultimately compiled in the testing program will allow the construction of analytical models to predict fracture properties as a function of material properties and test conditions. In addition, the models will include statistical analysis to construct confidence and tolerance intervals for the predicted values of fracture toughness. The results of this program may be used to disposition specific flaws in tank plates and thereby possibly reduce unnecessary conservatism

inherent in using lower bound properties and provide an improved safety envelope.

An evaluation of the effects of service on the A285 steel, and an initial compilation of mechanical properties for 1950's vintage A285 steel was previously reported.[1] It was determined that the fracture toughness of A285 steel was highly dependent on material specifications and loading conditions. Variables relevant to the material and load conditions for storage tanks were defined (as shown in Table 1) and a statistical test matrix was designed for mechanical testing (i.e. fracture toughness testing and tensile testing). Each of the variables was designated as a continuous (Cont.) or discrete (Disc.) variable in the statistical response surface model. Fracture toughness testing was done in the form of J-R fracture toughness curves. The test design consisted of seven variables that were expected to influence mechanical properties. Fracture toughness tests conducted in the first set focused on orientation (with respect to rolling direction) effects on fracture toughness specimens tested quasi-statically. The testing was limited to one heat of steel. This heat, Heat E400, was chosen as the compositionally (with a carbon content of 0.18%) bounding heat. Those results have previously been reported.[2]

Table 1: Test Matrix Variable Description

| Variable | Type | Span | |
|---|---|---|---|
| **Temp** | Cont. | 60°F | 80°F |
| **C Content** | Cont. | 0.08 wt% | 0.29 wt% |
| **Mn Content** | Cont. | 0.35 wt% | 0.9 wt% |
| **S Content** | Cont. | 0.005 wt% | 0.04 wt% |
| **Strain Rate** | Disc. | QS | Dyn. |
| **Orientation** | Disc. | L-T | T-L |

Recent fracture toughness testing included development of test procedures for dynamic strain rate fracture toughness testing. The results of recent fracture toughness testing, including 11 quasi-static and 6 dynamic strain rate tests, are reported. In addition, possible individual variable influences on fracture toughness properties of A285 steel are discussed. A comparison of fracture toughness properties of modern steel vs. archival steel is also made.

## MATERIALS

Material was selected to closely match the materials used in storage tanks used at Savannah River Site. The carbon steel material for storage tanks was fabricated per specification ASTM A285-50T, Grade B firebox quality (A285). A total of 12 heats were selected from various manufacturers. The heats were chosen on the basis of their chemical composition, but were also limited by commercial availability. Grade C material was obtained when Grade B materials were unavailable. Grade C materials differed only slightly in strength and were more readily available than Grade B materials. These heats were produced of semi-killed, hot rolled plate steel. In addition to the commercially obtained heats, heat "Adisk" represented archival steel found at the Savannah River Site. Heat Adisk has no other pedigree other than recent on-site compositional analysis. Of the twelve total heats, the heats recently tested are shown Table 2 with their chemical compositions (i.e. carbon, manganese, and sulfur content), plate thickness, supplier, and tensile properties (i.e. ultimate tensile strength, yield strength, and elongation).

Table 2: Materials Tested including Tensile Properties, Chemical Composition, and Plate Thickness.

| Heat | B (in.) | C | Mn | S | $S_{UTS}$ (ksi) | $S_{Y\ (0.2\%)}$ (ksi) |
|---|---|---|---|---|---|---|
| **P134** | 1.125 | 0.083 | 0.854 | 0.032 | 60 | 40 |
| **1A434** | 0.875 | 0.082 | 0.676 | 0.011 | 64 | 46 |
| **R0296** | 1 | 0.16 | 0.53 | 0.01 | 67 | 42 |
| **A3184** | 0.625 | 0.1 | 0.86 | 0.013 | 60 | 41 |
| **Adisk** | 1.125 | 0.23 | 0.42 | 0.027 | 65 | 34 |

## TESTING

The conditions and heats selected for fracture toughness testing in FY00 (as part of the complete test matrix) are presented in Table 3. Fracture toughness testing concentrated primarily on effects of loading rate, thickness, and chemical composition. A total of 17 fracture toughness tests, in the form of J-R curve testing, were completed in the recent set as a part of the complete test matrix. The complete test matrix consists of 108 tests.

Table 3: Fracture Toughness Test Matrix as part of Complete Test Design

| SAMPLE | Thick. (in.) | T (°F) | Loading Rate | Or. |
|---|---|---|---|---|
| *P134-2* | 0.85 | 80 | Quasi-Static | T-L |
| *P134-3* | 0.85 | 80 | Dynamic | T-L |
| *P134-6* | 0.875 | 60 | Quasi-Static | T-L |
| *ADisk-1* | 0.875 | 60 | Dynamic | T-L |
| *ADisk-2* | 0.875 | 60 | Quasi-Static | T-L |
| *ADisk-3* | 0.875 | 80 | Dynamic | T-L |
| *ADisk-4* | 0.875 | 80 | Quasi-Static | T-L |
| *1A434-1* | 0.476 | 70 | Dynamic | T-L |
| *1A434-3* | 0.625 | 60 | Quasi-Static | T-L |
| *1A434-5* | 0.852 | 80 | Quasi-Static | T-L |
| *R0296-1* | 0.476 | 60 | Quasi-Static | T-L |
| *R0296-5* | 0.65 | 80 | Quasi-Static | T-L |
| *R0296-8* | 0.876 | 70 | Quasi-Static | T-L |
| *A3184-1* | 0.476 | 60 | Quasi-Static | T-L |
| *A3184-4* | 0.476 | 60 | Dynamic | T-L |
| *A3184-5* | 0.602 | 80 | Quasi-Static | T-L |
| *A3184-7* | 0.601 | 80 | Dynamic | T-L |

The standard method for J-integral characterization described in ASTM Standard E1820: "Standard Test Method for Measurement of Fracture Toughness" was followed for fracture toughness testing and development of J –Δa curves.[3] Fracture toughness tests were conducted on compact tension specimens machined to ASTM E1820 specifications. However, an extended width ('W') was used to allow for back end constraint and for measurement of fracture energy 'J' at large crack extensions. The specimens were 20% side-grooved to prevent extensive crack tunneling. The specimens were fatigue-precracked according to ASTM E1820 specifications. The quasi-static and dynamic loading rates (load-line displacement rates) were $1.24 \times 10^{-4}$ in/sec and 0.11 in/sec respectively. Testing was conducted at 60°F, 70°F, and 80°F, in an MTS™ Controlled Temperature Cabinet with temperature control to 1°F, nominally to reflect operational conditions of the storage tanks.

## Compact Tension Test

Fracture toughness testing was done on an MTS™ hydraulic load frame in a temperature controlled test chamber (shown in Figure 1). Temperature was measured/monitored using a calibrated temperature probe and the test chamber controller thermocouple during testing. Load, load-line displacement and crack lengths were measured for calculation of J-Δa curves. A crack-opening displacement (COD) gage was used to measure displacement up to 0.5 inches. Load-line displacement was measured through the MTS controller at greater crack openings to allow for extensive crack opening during testing. The compliance of the machine was not accounted for in the initial data analysis, resulting in an artificially high displacement for a given load/stress.

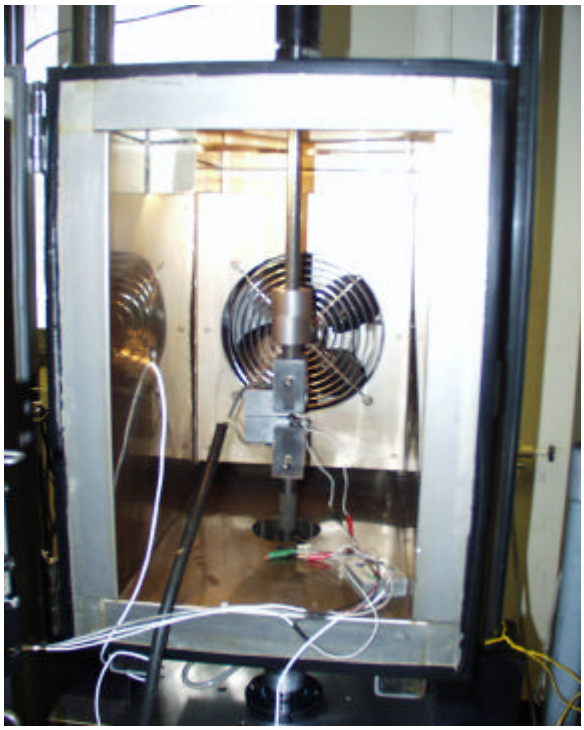

Figure 1: Specimen Setup in Test Chamber with Crack Length Potential Drop Measurement System

Crack lengths were measured using the Direct Current Potential Drop Method (DCPD). The specimen was instrumented as described in ASTM E647-95a, "Standard Test Method for Measurement of Fatigue Crack Growth Rates."[4] Calibration curves were developed on specimens prepared with different starting crack lengths.

Dynamic fracture testing (rapid-load testing) covered intermediate loading rates between quasi-static and impact Charpy tests. A sample geometry-specific (i.e. thickness) calibration curve was developed to provide a linear relationship between crack length and measured current potential drop. It was determined that thickness variations affected only the initial voltage and not the linear relationship. As a result crack length measurements from each of the samples were identically calibrated. Voltage output from the direct current potential drop system was monitored using Labview™ data acquisition

software. A data sampling rate of 500 samples/sec was chosen to maximize crack length measurement accuracy while ensuring a sufficient number of data points in the vicinity of crack initiation to enable accurate J calculations at crack initiation. The DCPD results were calibrated with post-test optical crack length measurements of the fatigue pre-crack and total crack length after testing.

## RESULTS AND DISCUSSION

Fracture resistance curves, in the form of J-Δa curves, were developed for each of the tests. The material fracture toughness curve characterizes its resistance to: (1) fracture of a stationary crack, (2) fracture onset after some stable tearing, (3) stable tearing onset, and (4) sustained stable tearing. Unstable crack extension (i.e., significant pop-in) and fracture instabilities are indicated on the appropriate curves. Stable crack extension (i.e. "stable tearing") is to be otherwise assumed. In general, these materials exhibit a high toughness in the test temperature range. In most cases, crack growth did not initiate before the specimen underwent significant plastic deformation in the pre-cracked region and stable crack growth was accompanied by growth of the plastic zone ahead of the crack front.

A figure-of-merit of J at 3mm (0.118 in.) of crack extension was selected to provide a point of comparison of results from the J-Δa curves. A crack extension of 3 mm is approximately the boundary for valid crack length and J fracture energy measurements as defined by the ASTM E1820 construction. The figure-of-merit of the extended crack length of 3mm was chosen for accreditation of sustained stable tearing. This is of particular importance during J-T calculations of structural integrity. Utilizing $J_{3mm}$ as the material property allows for ductile tearing whereas using $J_{Ic}$ credits only for crack initiation toughness.

The following sections will briefly discuss the observed effect of each of the matrix variables. It is important to note that the statistical test matrix does not allow isolation of variables, but accounts for variable-specific fracture toughness with an applied confidence. The presented results are preliminary and a better assessment of the impact of each matrix variable will be made once the testing program is complete. The statistically designed test matrix and the quadratic model that will be used to accurately predict the effect of each of these variables, will account for variable interaction when the matrix is complete. However when considering the current available data set, numerous trends may be proposed. Previously reported testing results will also be used to hypothesize interim conclusions.

### Effect of Test Temperature

The effect of temperature on the fracture energy of steels is well understood and documented.[5] In general, ferritic steels exhibit a ductile to brittle transition temperature (DBTT). Ferritic steels undergo a transition from ductile behavior (fracture by microvoid coalescence) at higher temperature to brittle behavior (fracture by cleavage) at lower temperature. The temperature range and magnitude of this transition are a complex function of composition, thermo-mechanical processing, strain rate and many other factors. From the current data set, it is difficult to observe any effect of temperature on fracture properties over the limited range tested. The effect of temperature seems to be within the variability of the material and/or measuring techniques. Previous testing has also indicated negligible temperature effects on fracture toughness over a similarly limited temperature range.[2]

Considering the narrow range of temperatures selected for testing in the present program, this implies that the present test temperatures fall above the DBTT of the steel heats. A dramatic test temperature effect would be evident in the fracture properties if the test temperatures fell within the transition range. It is important to note that the temperature effect may depend upon loading rate and specimen geometry. Additional tests in the dynamic loading regime will be performed as part of the complete test design to ascertain the effect of test temperature, as a function of loading rate, on the fracture toughness of these steels. Calculated values of $J_{3mm}$ from experimental data for all tests to date are shown as a function of test temperature and loading rate in Figure 2. All other variables are not considered for purposes of this graph.

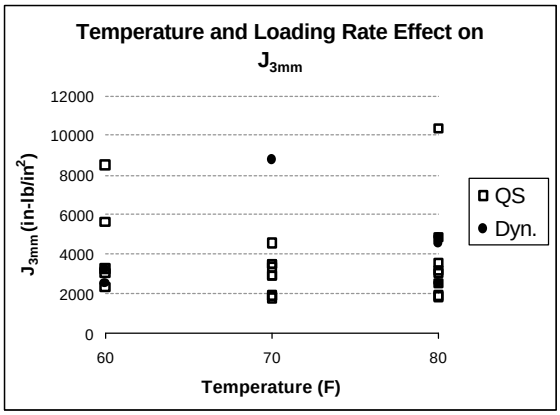


Figure 2: $J_{3mm}$ as a Function of Test Temperature and Loading Rate (including all test results).

## Effect of Steel Heat Composition

The compositional variables most commonly expected to play a role in determining fracture toughness properties and modes in low carbon steels are carbon content, manganese content, and sulfur content. In low carbon steels, carbon is typically present as either grain boundary carbides, pearlite, or spherical carbides depending on the carbon level and heat treatment. The mechanism of strengthening depends on the form of carbon present, the size of those constituents, the distribution, and their spacing. Manganese strengthens steel by solution strengthening the $\alpha$-iron matrix and is also effective in gettering free sulfur via the production of MnS inclusion. Inhomogeneity of Mn may result in a banded ferrite/pearlite structure. Free sulfur may segregate to grain boundaries, while both MnS and iron sulfides may be present depending on the compositional heat treatment. MnS is generally poorly bonded to the host matrix and these inclusions act as nucleation sites for void formation and are considered to increase transition temperature of steels.

It is difficult to isolate the influence of one compositional variable with respect to the other, since they cannot be isolated from each other. Several general observations, with respect to compositional influence on fracture properties, can be made from the data collected in the present study. The magnitude of fracture energy with extended crack growth appears to decrease with increasing carbon content and decreasing manganese content.

Increased pearlite content has been shown to reduce the fracture energy in steels. Increased carbon content generally produces a higher volume fraction of pearlite, which is important in ductile fracture and sub-critical crack growth. There has been considerable work done on the microstructural parameters controlling the flow and fracture of pearlite.[6,7] The cracking of pearlite colonies initiates voids as the surrounding ferrite matrix flows plastically around them.[8] Ductile fracture occurs by coalescence of these voids. The mechanical properties are also dependent on the interlamellar spacing of the pearlite. The extent of pearlitic banding resulting from Mn segregation also affects the crack path selection and fracture resistance. Since the steel heats with higher carbon content have a higher volume fraction of pearlite, subcritical crack growth is facilitated under quasi-static loading. As a result, the magnitude of fracture energy is lower at extended crack growth in the heats of steel with higher carbon content.

Each of these tests was done at the quasi-static loading rate. Figure 3 shows data from all of the tests performed. There is a great deal of scatter and even higher values as done by other tests, once again disregarding all other variables. The scatter may be due to the interaction of various variables. There does not appear to be any correlation between the Mn/C ratio with the fracture energy at an extended crack length of 3mm in the data set collected.

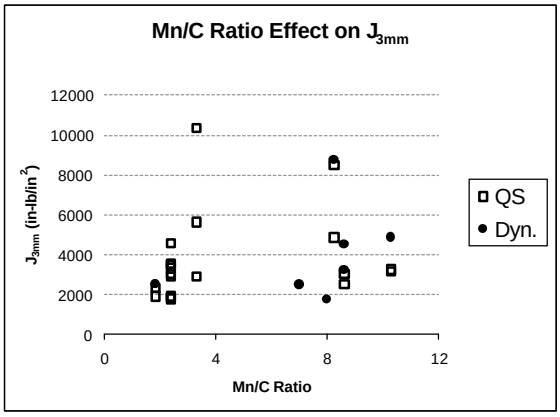


Figure 3: Manganese/Carbon Ratio Effect on $J_{3mm}$.

## Effect of Sample Geometry

The geometry of the compact tension specimen influences fracture properties by controlling stress state at the crack tip. The stress state of the compact tension sample during fracture toughness testing transitions from a plane stress to plane strain configuration with increasing thickness. In thicker specimens triaxial stresses predominate due to increased constraint across the thickness. The plastic zone size is consequently diminished and the fracture energy is reduced.

Specimen thickness in the current test program varied only between 0.5" and 0.875" to reflect the thickness of storage tanks in service. The thickness of the test samples were not enough to ensure plane strain conditions for A285 steel as per ASTM E1820. Therefore, the stress state during testing was expected to be varying degrees of plane stress and thickness was not expected to be a primary contributor to fracture energy results.

Fracture toughness curves from tests performed at quasi-static loading rates seem to indicate that the effect of thickness on fracture energy is within the variability of the material and/or measuring techniques. However, contrary to stress state variance, reducing thickness (by machining) may not increase toughness when large rolling defects are concentrated in the central portion of the plate's thickness. Machining away the outer surfaces of the plate would enhance the influence of these defects on the fracture energy. A comparison of thickness effects , disregarding other factors, on $J_{3mm}$ is shown in Figure 4.

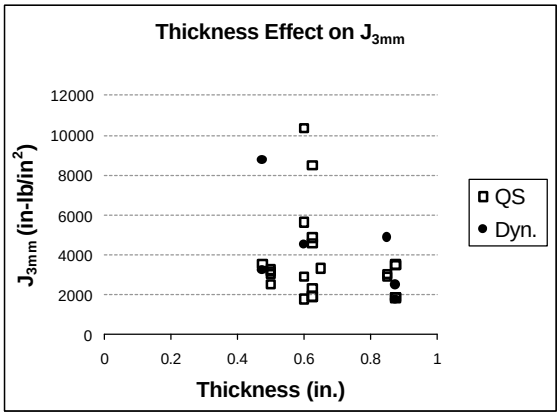


Figure 4: Sample Thickness Effect on $J_{3mm}$.

## Effect of Loading Rate

Specific J-Curves are shown in Figure 5 to show the strain rate effects on the fracture energy of recent vintage A285 steels as chosen from the recent testing. It is seen that, at the same test temperature, with the same specimen dimensions, the J fracture energy curve for the dynamic testing done on samples A3184-5 and P134-2 are higher in magnitude than their quasi-statically tested counterparts A3184-7 and P134-3. The load carrying capacity and the resistance to ductile tearing tend to increase with increasing loading rate. However, high strain rates may lead to the unexpected onset of cleavage fracture as will be discussed later.

The higher resistance to ductile tearing which presently accompanies the tests done at higher loading rates has several possible sources. It has been proposed that under dynamic loading rates, higher flow stress is required to attain the strain necessary for void coalescence.[9] Xia and Shih have observed a higher tensile stress in the fracture process zone ahead of the crack tip in highly strain rate sensitive materials. This has been proposed to lead to a high plastic dissipation and rapidly rising ductile tearing resistance curve which accompanies an increase in loading rate.[10]

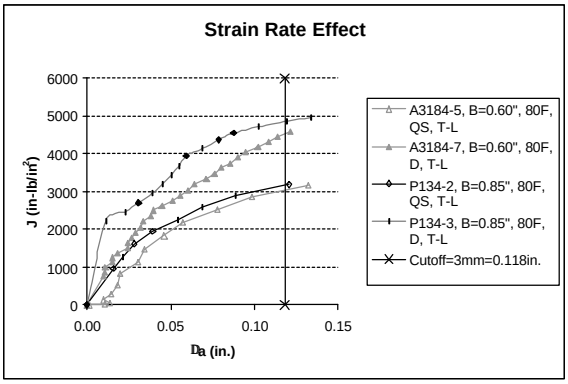


Figure 5: Strain Rate Effect on J Fracture Energy Curves of Specific Samples Tested of Recent Vintage A285 Steel

## Archival Material Testing

Test results of the archival material are shown in Figure 6. Both dynamic strain rate tests resulted in cleavage fracture at the maximum crack length shown (approximately 0.12"). Ductile tearing was the primary failure mechanism until that point and then was interrupted by the onset of catastrophic cleavage fracture. This type of cleavage fracture interruption is known to be a function of the microstructure, constraint, loading rate, and temperature. However, the curves are comparable until $J_{3mm}$. It is interesting to note that for the archival material, the load carrying capacity and the resistance to ductile tearing does not increase remarkably more rapidly in the dynamic strain rate tests than the quasi-static counterpart. This is in contrast to the testing done on the steels of recent vintage as previously mentioned. It is also clear that all J-Δa curves for the archival material shown in Figure 6 lie lower of those in Figure 5. Cleavage intervenes at a much lower J value for tests done on the archival material. It is expected that this is due to the high carbon content. The fracture toughness curves of Heat E400, also higher in carbon content, have the same lower magnitude for the quasi-static tests. Dynamic strain rate testing on Heat E400 will

be done to confirm the influence of high carbon content on the intervention of cleavage fracture.

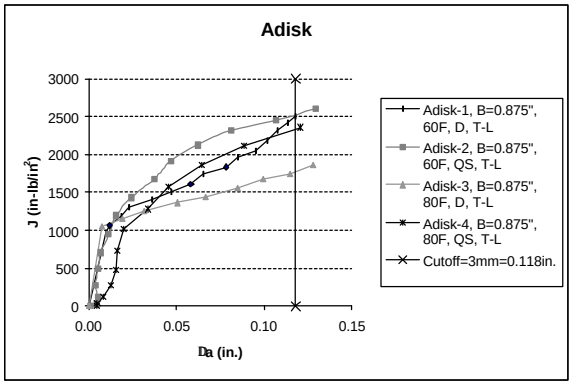


Figure 6: Heat Adisk J-Δa Fracture Toughness Curves.

The temperature effects are minimal in the range of temperatures tested. In this case, all samples were of the same geometry. Therefore, the loading rate is considered the only detrimental factor for these tests in the onset of cleavage fracture. At high loading rates, the probability of cleavage fracture intervention appears to be higher than at quasi-static rates. Ductile crack growth and the increase in energy required to propagate fracture may eventually be enough to trigger cleavage. At higher loading rates, the strength/flow stress of the material in the crack tip region is elevated. If this is elevated sufficiently to reach the cleavage fracture stress locally, rapid cleavage fracture may ensue. In addition, as more material is sampled due to the increased plastic zone size which accompanies ductile crack growth, in combination with the high strain rate, the probability of the crack tip encountering an inclusion or other brittle region to trigger cleavage fracture also increases.[10]

SEM fractographs of Adisk material (shown in Figure 7 and Figure 8 for samples Adisk-1 and Adisk-2 respectively) revealed ductile tearing that was interrupted by a cleavage instability. Higher magnification images showed that regions of brittle and ductile fracture coexist during stable crack growth in sample Adisk-1, which was tested in dynamic conditions. In contrast, Adisk 2, which was tested in quasi-static conditions, exhibited no evidence of brittle failure on the fracture surface and stable crack growth continued for over 0.4 inches without unstable crack growth occurring.

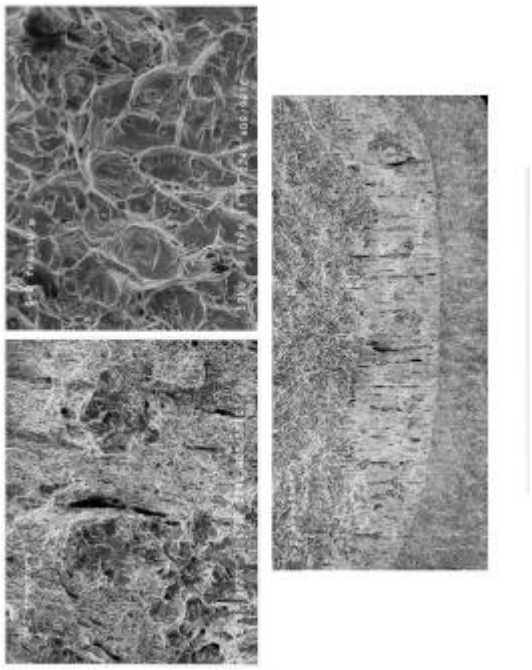

Figure 7: SEM Fractograph of Adisk1 Tested at 60 $^{o}$F at the Dynamic Loading Rate (T-L Orientation)

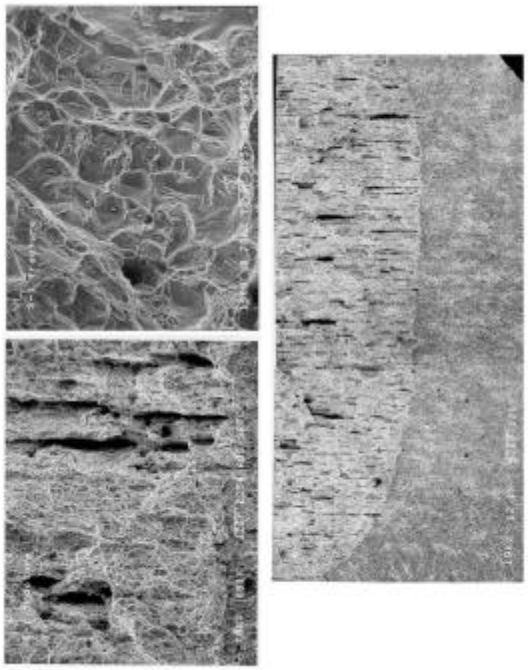

Figure 8: : SEM Fractograph of Adisk2 Tested at 60 $^{o}$F at the Quasi-static Loading Rate (T-L Orientation)

## CONCLUSIONS

The current results have permitted an initial evaluation of the effects of different variables on the fracture energy. It is shown that changes in test temperature and thickness in the ranges tested have minimal effects. The preliminary findings reveal that higher loading rates lead to more rapidly increasing J-curves in recent vintage low-carbon steels in comparison with quasi-static loading rates. However, for archival material, containing higher carbon contents, the effect is less pronounced. The onset of cleavage fracture after extended ductile tearing is also seen as a function of loading rate, as tests conducted on archival material isolated loading rate as a variable. The failure mechanism in these cases revealed the competition between ductile tearing and cleavage failure. The observation of cleavage onset after ductile tearing was seen to be higher at higher loading rates. The present tests highlight the continuing need to determine the allowable crack growth resistance as well as to quantify the ductile tearing to cleavage fracture transition.

## PATH FORWARD

Additional fracture toughness tests will be performed to complete the test matrix. Results from the complete data set will be used to determine the sensitivity of the predictive model to each matrix variable. Microstructural analysis will be conducted to develop a fundamental understanding of the role of microstructure on fracture energy and to determine more quantitative structure/property relationships. Finally, a phased approach to large-scale tests on actual tank materials will validate the application of the predictive property model.

## ACKNOWLEDGMENTS

This work was funded by the U. S. Department of Energy under contract No. DE-AC09-96SR18500.

## REFERENCES

1 Sindelar, R. L., Lam, P-S., Caskey, G. R., Woo, L. Y., “Flaw Stability in Mild Steel Tanks in the Upper-Shelf Ductile Range – Part 1: Mechanical Properties,” J. Pres. Ves. Tech., Vol. 122, pp. 162-168, May 2000.

2 Duncan, A. J., Subramanian, K.H., Sindelar, R. L., Wiersma, B. J., Miller, K., Reynolds, A. P., and Chao, Y. J., “J-Integral Fracture Toughness Testing and Correlation to Microstructure of A285 Steel for Fracture Analysis of Storage Tanks.”, ASME PVP Vol. 413, July 2000, p. 143-150.

3 "Standard Test Method for Measurement of Fracture Toughness,” American Society for Testing Materials Annual Book of Standards. Vol. 3.01 Standard E1820, 1999.

4 “Standard Test Method for Measurement of Fatigue Crack Growth Rates,” American Society for Testing Materials Annual Book of Standards. Vol. 3.01 Standard E647, 1999.

5 Burns, K. W., Pickering, F. B., “Deformation and Fracture of Ferrite-Pearlite Structures,” Journal of Iron and Steel Institute, November 1964, pp. 899-906.

6 Lewandowski, J. J., Thompson, A. W., “Micromechanisms of Cleavage Fracture in Fully Pearlitic Microstructures,” Acta Met., Vol. 35 No. 7, pp. 1453-1462, 1987.

7 Lewandowski, J. J., Thompson, A. W., “Microstructural Effects on the Cleavage Fracture Stress of Fully Pearlitic Eutectoid Steel,” Met. Trans. A., Vol. 17A, pp. 1769-1786, 1986.

8 Gurland, J., Plateau, J., “The Mechanisms of Ductile Rupture of Metals Containing Inclusions,” Trans. Am. Soc. Metals, Vol. 56, pp. 442-454, 1963.

9 Wilson, M. L., Hawley, R. H., Duffy, J., “The Effect of Loading Rate and Temperature on Fracture Initiation in 1020 Hot-Rolled Steel,” Engr. Fract. Mech., Vol. 13, pp. 317-385, 1980.

10 Xia, L, Shih, C. F., “Ductile Crack Growth – III. Transition to Cleavage Fracture Incorporating Statistics,” J. Mech. Phys. Solids, Vol. 44, pp 603-639, 1996.